Letter

Controlling nonequilibrium Bose-Einstein condensation with engineered environments

Francesco Petiziol [*] and André Eckardt [†]
Institut für Theoretische Physik, Technische Universität Berlin, Hardenbergstrasse 36, 10623 Berlin, Germany

(Received 9 November 2023; revised 12 March 2024; accepted 29 July 2024; published 23 August 2024)

Out of thermal equilibrium, bosonic quantum systems can undergo Bose condensation away from the ground state, featuring a macroscopic occupation of an excited state or even of multiple states in the so-called Bose-selection scenario. In previous work, a theory was developed that predicts in which states a driven-dissipative ideal Bose gas condenses. Here we address the inverse problem: Given a target state with desired condensate fractions in certain single-particle states, how can this configuration be achieved by tuning available control parameters? Which type of experimental setup allows for flexible condensation control? We solve these problems, on the one hand, by proposing a Bose condenser, experimentally implementable in a superconducting circuit, where targeted Bose condensation into eigenstates of a chain of resonators is driven through the coupling to artificial quantum baths, realized via auxiliary two-level systems. On the other hand, we develop a theory to solve the inverse problem based on linear-programming methods. We further discuss the engineering of transition points between different Bose condensation configurations, which may find application in amplification, heat-flow control, and the design of highly structured quantum baths.

DOI: 10.1103/PhysRevA.110.L021701

Introduction. Nonequilibrium Bose-Einstein condensation (BEC) has been widely explored in different platforms [1], such as photons in dye-filled cavities [2–8], excitons [9–11], and exciton polaritons [12–19] in (cavity) semiconductor heterostructures. Bose-Einstein condensation in these systems results from the interplay of thermalization with pump and loss, whose ratio determines the condensate mode. Nonequilibrium BEC of a different kind is predicted to occur, however, also at a conserved particle number, when other mechanisms deprive the ground state of its privileged role. Examples are open systems subject to time-periodic driving or to a strong competition between heating and cooling mechanisms [20–24]. Steady states with multiple condensates in Bose-selected modes arise here from the nonequilibrium quantum-jump kinetics. Controlling their (fragmented) condensation pattern on demand is an appealing perspective for the design of, e.g., quantum signal amplifiers, multimode emitters, structured artificial quantum baths, or heat-transport regulators. However, while a theory explaining Bose selection (BS) has been developed [20,21], approaches to systematically engineer nonequilibrium BS, turning it into a practical resource, are missing. The key challenges are (i) how to realize controllable quantum-jump networks in realistic experimental conditions and (ii) how to solve the inverse problem of finding values of the control knobs yielding a target BS configuration. In this work we solve both problems by proposing a concrete experimental setup where nonequilibrium BEC of photons can be controlled in a superconducting circuit using synthetic reservoirs and by developing methods to reverse engineer control parameters yielding desired condensation patterns. We demonstrate the success of this procedure in simulations with realistic values of experimental parameters and propose an application in the design of a quantum switch for heat transport.

Bose selection. Bose selection can occur in a system of N noninteracting bosons exchanging energy with its environment, whose dissipative dynamics is described by a many-body Lindblad master equation ($\hbar = 1$)

$$\dot{\hat{\rho}}_S = -i[\hat{H}_S, \hat{\rho}_S] + \sum_{ij} R_{ij} D[\hat{L}_{ij}]\hat{\rho}_S \tag{1}$$

for the density operator $\hat{\rho}_S$. Given single-particle eigenstates $|i\rangle$ with energy E_i, Eq. (1) involves the Hamiltonian $\hat{H}_S = \sum_i E_i \hat{n}_i$, dissipators $D[\hat{L}_{ij}]\hat{\rho}_S = \hat{L}_{ij}\hat{\rho}_S\hat{L}_{ij}^\dagger - \{\hat{L}_{ij}^\dagger \hat{L}_{ij}, \hat{\rho}_S\}/2$ with rates R_{ij} for quantum jumps from $|j\rangle$ to $|i\rangle$, jump operators $\hat{L}_{ij} = \hat{c}_i^\dagger \hat{c}_j$, and annihilation and number operators $\hat{c}_i$ and $\hat{n}_i = \hat{c}_i^\dagger \hat{c}_i$ for a boson in the ith single-particle state. The rates are assumed to realize a fully connected network, implying a unique steady state [20], which becomes the equilibrium state, only when $R_{ji}/R_{ij} = \exp[-\beta(E_i - E_j)]$, with inverse temperature β. Although the bosons are noninteracting, the coupling to the bath(s) makes the problem interacting, as the dissipator is quartic in the $\hat{c}_i$. The hierarchy of equations for the m-point correlators $\mathrm{tr}[\hat{\rho}_S \hat{n}_{i_1} \hat{n}_{i_2} \cdots \hat{n}_{i_m}]$, resulting from this interacting problem, can be truncated through a mean-field approximation, which yields nonlinear kinetic equations of motion for the $n_i = \mathrm{tr}(\hat{\rho}_S \hat{n}_i)$, namely, $\dot{n}_i = \sum_j [R_{ij} n_j (1 + n_i) - R_{ji} n_i (1 + n_j)]$ [20,21] [see the Supplemental Material (SM) [25] for a brief review]. The nonlinearity is related to Bose statistics, giving rise to a dependence of the many-body rate on the occupation of the state a particle jumps to, known as bosonic enhancement (or stimulated emission). It is responsible for the emergence

[*] Contact author: f.petiziol@tu-berlin.de
[†] Contact author: eckardt@tu-berlin.de

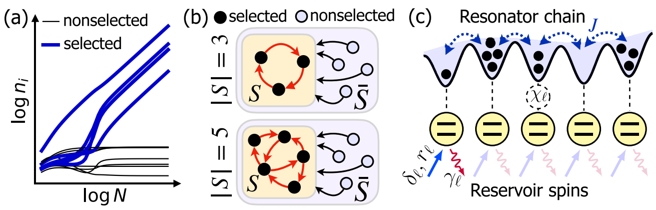

FIG. 1. (a) Sketch of the BS effect. Selected states acquire a macroscopic occupation proportional to N, while the occupation of nonselected states saturates for large N. (b) Network representation of examples of asymmetry matrices A compatible with BS (proof in the SM [25]). (c) Sketch of a Bose condenser. A resonator chain (blue), where BEC occurs in selected eigenmodes, is dispersively coupled to driven-damped reservoir two-level systems (yellow).

of BS in the steady state, satisfying $\dot{n}_i = 0$, where a single or multiple selected states acquire a macroscopic occupation proportional to N in the large-N limit, while the occupation of all other states saturates [sketch in Fig. 1(a)]. The set of selected states S (and its complement $\bar{S}$) can be predicted by considering a large-N expansion $n_i = \nu_i N + \sum_{\alpha=1}^{\infty} \nu_i^{(\alpha)}/N^{\alpha-1}$. This reveals that condensation is ruled, in leading order, by the rate-asymmetry matrix $A_{ij} = R_{ij} - R_{ji}$ through the set of (in)equalities [20,21]

$$A_{\bar{S}S}\boldsymbol{\nu}_S < 0, \quad A_{SS}\boldsymbol{\nu}_S = 0, \quad \boldsymbol{\nu}_{\bar{S}} = 0, \quad \boldsymbol{\nu}_S > 0, \tag{2}$$

which ensure that $n_i \geqslant 0$ for all i. The inequalities are understood elementwise and ν_X and A_{XY} denote subvectors and matrix blocks, respectively, with $X, Y \in \{S, \bar{S}\}$.

By depicting A as a network with edges pointing from the jth to the ith node if $R_{ij} > R_{ji}$, as in Fig. 1(b), physical intuition about rates R_{ij} admitting BS can be gained. The first condition in (2) is satisfied, e.g., if all nonselected states directly feed selected states, pointing at them in the network. Selection in a single state $|c\rangle$ occurs if and only if $R_{cj} > R_{jc}\,\forall\, j$ [20], thus making $|c\rangle$ ground-state-like. For multimode BS, no state in S must be a global attractor, as imposed by the second condition, demanding A_{SS} to have a nontrivial kernel vector $\nu_{S,i} > 0$. For three-state selection, this is possible only for a looplike configuration as in Fig. 1(b) (top) [25,33]. For larger sets S, more complex network topologies and rate imbalances are needed, with an example for $|S| = 5$ in Fig. 1(b) (bottom), and the resulting condensate fractions depend nonlinearly on A_{SS} [33,34] (and not only on the topology of the directed network). This highlights the difficulty in engineering specific condensation patterns, seemingly requiring one to assemble intricate rate networks edge by edge, which is beyond experimental reach. We therefore consider the more realistic scenario, where the rates depend on a number of control parameters, and show how these parameters can be optimized for achieving the desired BS pattern.

A superconducting Bose condenser. We propose an experimental implementation given by an array of M microwave resonators in a superconducting circuit [35–41]. Each resonator is dispersively coupled to an ancillary transmon qubit subject to coherent driving and loss, which implements a narrowband artificial bath (hereafter described by a spin 1/2) [Fig. 1(c)]. Owing to the harmonicity of the resonator spectrum, the array hosts noninteracting microwave photons [40], whose condensation we aim to control. The dynamics is described by the master equation

$$\frac{d\hat{\rho}}{dt} = -i[\hat{H}_S + \hat{H}_B + \hat{H}_{SB}, \hat{\rho}] + \sum_{\ell} \gamma_\ell D[\hat{\sigma}_\ell^-]\hat{\rho} \tag{3}$$

for the density matrix $\hat{\rho}$ of the combined resonator-spin system, where γ_ℓ is the decay rate of the ℓth spin and $\hat{\sigma}_\ell^\alpha$ $(\alpha = x, y, z, \pm)$ are Pauli matrices. The Hamiltonian $\hat{H}_S$ of the bosonic system is given by $\hat{H}_S = \sum_\ell \omega_\ell \hat{a}_\ell^\dagger \hat{a}_\ell - \sum_{\ell,\ell'} J_{\ell\ell'} \hat{a}_\ell^\dagger \hat{a}_{\ell'} = \sum_i E_i \hat{c}_i^\dagger \hat{c}_i$, where $\hat{a}_\ell$ and $\hat{a}_\ell^\dagger$ are the annihilation and creation operators of a photon in the ℓth resonator, respectively, which has transition frequency ω_ℓ, and $J_{\ell\ell'} > 0$ are the tunneling strengths. We choose the example of $\hat{H}_S$ describing a one-dimensional chain, with $J_{\ell\ell'} = J$ for nearest neighbors ℓ and ℓ'. We include a weak disorder $|\omega_\ell - \omega_{\ell'}| \sim J_{\ell\ell'}$ to break symmetries inducing multiple identical level spacings in the spectrum. Concretely, we use $\omega_\ell/J = \ell/10 + \varepsilon_\ell$, where ε_ℓ are random numbers uniformly distributed in [0,1) [25], though the specific values are not important for the target physics. These values of ω_ℓ are also chosen such that the eigenmodes $|i\rangle$ are still delocalized over several lattice sites for the system sizes considered. These features will be useful for realizing efficient dissipation engineering. The artificial-bath Hamiltonian $\hat{H}_B = \sum_\ell \delta_\ell(\hat{\sigma}_\ell^z + r_\ell \hat{\sigma}_\ell^x)/2$ describes the transmon spins (in a frame rotating at the driving frequency), where δ_ℓ is the detuning of the drive and r_ℓ is the ratio between its Rabi frequency and δ_ℓ. In the dispersive-coupling regime, the spins are far detuned from the resonators. Resonant exchange of excitations is thus strongly unfavored, implying photon-number conservation as desired (weak particle loss is discussed later). Other system–artificial-bath couplings as used, e.g., in Refs. [39,42] would involve particle exchange instead. Moreover, in the dispersive regime, undesired photon-photon interactions induced by the coupling to the spins can also be neglected. The resonator-spin coupling is described by the Hamiltonian $\hat{H}_{SB} = \sum_\ell \chi_\ell \hat{a}_\ell^\dagger \hat{a}_\ell \hat{\sigma}_\ell^z$, provided the mean number of photons in a resonator does not exceed a critical value [36,43]. For the parameters used below, tens to hundreds of photons per site are allowed, sufficient for BS. Condensation control will be achieved through the coherent drive and by tuning the value of the dispersive coupling χ_ℓ, in order to leverage the impact of each artificial bath on the quantum-jump network. Control of χ_ℓ is implemented, for instance, with frequency-tunable transmons, by adapting their detuning from the resonators [44,45], or ones with tunable coupling [46,47]. Note that the use of nonlinear (two-level) elements as the artificial bath, rather than additional cavity modes [48–51], is crucial: The dispersive coupling to the latter would only give a mutual state-independent energy shift [36], rather than the density-density-like coupling in $\hat{H}_{SB}$.

Engineered quantum-jump rates. Although $\hat{H}_{SB}$ commutes with the boson number $\hat{a}_\ell^\dagger \hat{a}_\ell$ in a single resonator, preventing particle loss, it has sizable matrix elements between the non-site-local modes $|i\rangle$, giving rise to nonzero off-diagonal elements of R_{ij} tunable via the spins. Intuitively, this enables dissipation engineering with the following mechanism. The coherent-control parameters δ_ℓ and r_ℓ are adapted such that the spin's excitation energy $\mathcal{E}_\ell = \delta_\ell\sqrt{1 + r_\ell^2}$ matches the energy spacing between states $|i\rangle$ and $|j\rangle$ in the array.

The coupling drives a coherent excitation exchange involving an $|i\rangle \leftrightarrow |j\rangle$ transition, with a matrix element $\chi_{ij}^{(\ell)} = r_\ell \chi_\ell M_{ij}^{(\ell)}/\sqrt{1+r_\ell^2}$, where $M_{ij}^{(\ell)} = \langle i|\,\hat{a}_\ell^\dagger \hat{a}_\ell\,|j\rangle$, which we compute below. This excitation flip-flop is interrupted by the strong spin damping, which drags the spin to its drive-dependent steady state and results in dissipative quantum jumps in the bosonic chain at rates R_{ij} and R_{ji}. Here the spin relaxation time plays a role similar to a short bath correlation time in the more conventional Born-Markov scenario with a large bath.

To derive the rates $R_{ij} = \sum_\ell R_{ij}^{(\ell)}$ of Eq. (1) from Eq. (3), consider first a single reservoir spin coupled to the ℓth resonator (further technical details on the derivation are given in the SM [25]). The generalization to multiple reservoirs is straightforward, as their rates simply sum up. Representing Eq. (3) in a diagonal basis for the spin, terms corresponding to nonsecular (off-diagonal) elements of the Kossakowski matrix of the dissipator are off-resonant and can be neglected in the rotating-wave approximation (RWA). This is justified provided the spin level splitting $|\mathcal{E}_\ell|$ is much larger than its decay rate γ_ℓ, namely, $|\mathcal{E}_\ell| \gg \gamma_\ell$ (approximation I). Equation (3) becomes

$$\dot{\hat{\rho}} = -i\left[\sum_i E_i \hat{n}_i - \sum_{i,j} \chi_{ij}^{(\ell)} \hat{L}_{ij}\left(\frac{\hat{\sigma}_\ell^z}{r_\ell} + \hat{\sigma}_\ell^x\right) - \frac{\mathcal{E}_\ell}{2}\hat{\sigma}_\ell^z, \hat{\rho}\right] + \gamma_\ell^+ D[\hat{\sigma}_\ell^+]\hat{\rho} + \gamma_\ell^- D[\hat{\sigma}_\ell^-]\hat{\rho} + \gamma_\ell^z D\big[\hat{\sigma}_\ell^z\big]\hat{\rho}, \tag{4}$$

including $\mathcal{E}_\ell = \delta_\ell\sqrt{1+r_\ell^2}$ and the dressed decay rates $\gamma_\ell^+ = \gamma_\ell \cos(\theta_\ell)^4$, $\gamma_\ell^- = \gamma_\ell \sin(\theta_\ell)^4$, and $\gamma_\ell^z = \gamma_\ell r_\ell^2/4(1+r_\ell^2)$, where $\theta_\ell = \arctan(r_\ell)/2$ is the spin's mixing angle.

Considering the case in which $\mathcal{E}_\ell$ is (quasi)resonant with the level spacing $E_{ij} = E_i - E_j > 0$ in the system, the interaction terms $\hat{L}_{ij}\hat{\sigma}_\ell^+$ and $\hat{L}_{ij}^\dagger\hat{\sigma}_\ell^-$ become resonant. Other interaction terms can be neglected, in the RWA, if E_{ij} is much larger than the effective coupling $\chi_{ij}^{(\ell)}$, $E_{ij} \gg |\chi_{ij}^{(\ell)}|$ (approximation II). Next we trace out the spin, treating it as an environmental degree of freedom, with $\chi_{ij}^{(\ell)}$ representing a system-bath coupling, and following standard Born-Markov-secular derivations [52]. This approach is justified, despite the spin being far from constituting a true bath, provided the spin relaxes much faster than the timescale of interaction with the system, $|\chi_{ij}^{(\ell)}| \ll \gamma_\ell$ (approximation III). Then the spin state is negligibly affected by this interaction and can be approximated as constant. Moreover, the state of the system and the artificial bath can be approximated as factorized. The dynamics of the system is then described by the Markovian master equation [52] $\dot{\hat{\rho}}_S = \int_0^{+\infty} ds\, \mathrm{tr}_\sigma[\hat{H}(t), [\hat{H}(t-s), \hat{\rho}_S \otimes \hat{\rho}_\sigma]]$, where tr_σ and $\hat{\rho}_\sigma$ denote the trace over the spin degrees of freedom and the spin's steady state, respectively, and $\hat{H}(t)$ represents the Hamiltonian of Eq. (4) in the interaction picture.

Following standard manipulations [52], the Markovian master equation can be brought into the form of Eq. (1), within approximations I–III, with rates $R_{ij}^{(\ell)} = |\chi_{ij}^{(\ell)}|^2 \mathcal{S}_\ell^+(-E_{ij})$ and $R_{ji}^{(\ell)} = |\chi_{ij}^{(\ell)}|^2 \mathcal{S}_\ell^-(E_{ij})$ for $\delta_\ell > 0$. The quantum noise spectra $\mathcal{S}_\ell^\pm(\omega) = \int_{-\infty}^{\infty} dt\, e^{i\omega t}\mathrm{tr}\{[\hat{\sigma}_\ell^\pm(t)]^\dagger \hat{\sigma}_\ell^\pm(0)\hat{\rho}_\sigma\}$ are computed from the spin's steady state $\hat{\rho}_\sigma$ and the correlation functions.[1] Here the operators $\hat{\sigma}_\ell^\pm(t)$ are interaction-picture representations of $\hat{\sigma}_\ell^\pm$. The correlation functions are computed in the SM [25] from the optical Bloch equations for the spin and the quantum regression theorem [26,52]. We obtain the quantum noise spectra

$$\mathcal{S}_\ell^\pm(\omega) = \frac{\gamma_\ell^\mp}{\gamma_\ell^+ + \gamma_\ell^-}\frac{2\Gamma_\ell}{(\omega \pm \mathcal{E}_\ell)^2 + \Gamma_\ell^2}, \tag{5}$$

characterized by a linewidth $\Gamma_\ell = (\gamma_\ell/4)[3 - 1/(1+r_\ell^2)]$. For a positive $E_{ij} > 0$ and detuning $\delta_\ell > 0$, the rates can be rewritten as

$$R_{ij}^{(\ell)} = \gamma_\ell^-\big|\chi_{ij}^{(\ell)}\big|^2 \mathcal{S}_\ell(E_{ij}), \quad R_{ji}^{(\ell)} = \gamma_\ell^+\big|\chi_{ij}^{(\ell)}\big|^2 \mathcal{S}_\ell(E_{ij}), \tag{6}$$

with $\mathcal{S}_\ell(\omega) = 2\Gamma_\ell/[(\omega - |\mathcal{E}_\ell|)^2 + \Gamma_\ell^2]$. For $\delta_\ell < 0$, the rates have the same form (6), but with $\gamma_\ell^\pm$ exchanged. The driven spin dynamics determines the quantum-jump ratio $R_{ij}^{(\ell)}/R_{ji}^{(\ell)} = \gamma_\ell^-/\gamma_\ell^+ = \tan(\theta_\ell)^4$ via the mixing angle θ_ℓ. For $\delta_\ell > 0$ and $\theta_\ell \ll 1$, the spin dissipator in Eq. (4) drags the spin to its ground state, favoring the processes $\hat{L}_{ij}\hat{\sigma}_\ell^+$ that increase the system energy but blocking the inverse processes $\hat{L}_{ij}^\dagger\hat{\sigma}_\ell^-$ that lower the energy. The opposite occurs for $\theta_\ell \approx \pi/2$. Intermediate values of θ_ℓ allow both processes with a finite rate and are optimal to ensure a sizable matrix element $\chi_{ij}^{(\ell)} \propto r_\ell$, while complying with the weak-driving regime desired in experiments. Summarizing, each artificial bath can be tuned to increase or decrease the system energy with a controllable rate ratio and the corresponding rates are enhanced around the peak of $\mathcal{S}_\ell(\omega)$. Alternative control scenarios based on a Floquet modulation of the bosonic system may be possible, but would make the control more difficult. Indeed, strong driving alters the shape of the modes $|i\rangle$, which become Floquet states, and gives rise also to sideband quantum jumps (see, e.g., Refs. [20,24]).

The validity of Eq. (6) requires the hierarchy $E_{ij} \gg \gamma_\ell \gg |\chi_{ij}^{(\ell)}|$ between the system energy gap E_{ij}, the spin decay rates γ_ℓ, and the transition matrix elements $\chi_{ij}^{(\ell)}$, resulting from approximations I–III. This hierarchy defines the operating regime of the proposed Bose condenser, which is easily met in state-of-the-art superconducting devices [39]. In particular, we envision implementations involving a number of resonators of the order of 10, each coupled to a superconducting qubit, which are close to the setup of recent experiments [38,39] and suffice for the potential applications described below. Given that system gaps are of the order of the tunneling strength J for such system sizes, we may choose a value $J/2\pi \sim 30$ MHz and decay rates $\gamma_\ell \sim$ 1–10 MHz (realized, e.g., in [39]). The Rabi frequencies $|\delta_\ell| r_\ell$ used in our examples are lower than $1.5J \sim 2\pi \times 40$ MHz in value, thus meeting standard constraints for microwave drives on transmons. We then obtain $|\chi_{ij}^{(\ell)}| \sim 10^{-1}J$ by also restricting χ_ℓ to a maximal value $\chi_{\max} \sim 0.15J \sim 2\pi \times 4.5$ MHz [35]. In turn, this yields engineered quantum-jump rates $R_{ij} \sim 10^{-2}J$,

[1]For negative detuning, $\delta_\ell < 0$, the derivation of the master equation is the same as above, only with the role of $\hat{\sigma}_\ell^-$ and $\hat{\sigma}_\ell^+$ [and thus $\mathcal{S}_\ell^-(\omega)$ and $\mathcal{S}_\ell^+(\omega)$] exchanged.

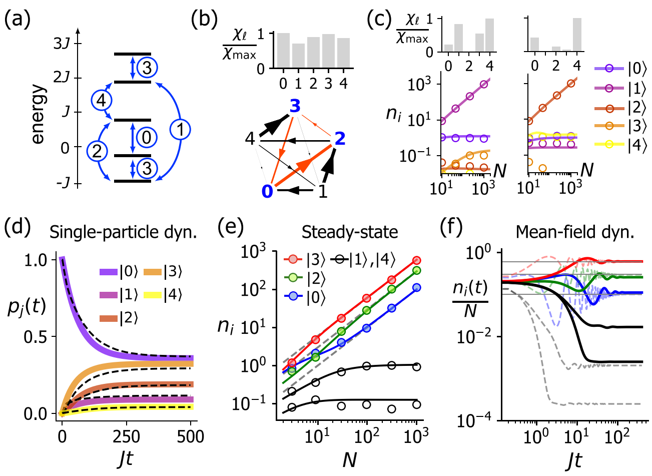

FIG. 2. (a) Single-particle spectrum of the five-site chain. The arrows with numbers indicate the reservoir spin used to induce the dissipative transition between the corresponding linked states. (b) and (d)–(f) Controlled BS in states $|0\rangle$, $|2\rangle$, and $|3\rangle$, namely, (b) the values of the control parameters χ_ℓ and the resulting asymmetry-matrix network [the arrows and their thickness represent $\mathrm{sgn}(A_{ij})$ and $|A_{ij}|$, respectively], (d) the single-particle dynamics, (e) the steady state as a function of the total particle number N, and (f) the mean-field dynamics for $N = 50$ (solid line) and $N = 500$ (dashed line). Symbols and line types are explained in the text. (c) Controlled BEC into single modes $|1\rangle$ and $|2\rangle$, and corresponding values of χ_ℓ.

much stronger than typical photon loss rates for microwave resonators in circuit QED [36]. Even in case losses are not compensated for (as we propose below), the system can thus form a Bose-selected steady state well before serious particle loss occurs.

Programmable BECs. To convert BS into a control problem in the Bose condenser, we identify controllable coefficients z leveraging the different bath contributions as $z_\ell = \mathrm{sign}(\delta_\ell)(\chi_\ell/\chi_{\max})^2$, leading to a decomposition of the total asymmetry matrix as $A = \sum_\ell z_\ell A^{(\ell)}$. We then construct a recipe to reverse engineer a z giving a target BS pattern $\boldsymbol{\nu}$. From the conditions (2) we derive a new set of inequalities for z,

$$(Bz)_{\bar{S}} < 0, \quad (Bz)_S = 0, \tag{7}$$

with $B_{ij} \equiv \sum_{\ell \in S} A_{i\ell}^{(j)} \nu_\ell$. If a solution z exists, it will stabilize the targeted steady state with $\boldsymbol{\nu}$ by construction. To efficiently search for solutions of Eqs. (7), we rephrase the inequalities as constraints in a linear program and solve them using linear-programming routines [25,33]. This procedure represents a powerful framework to reverse engineer BS patterns. Let us exemplify it by considering a five-site chain, possessing the single-particle spectrum shown in Fig. 2(a). The specific values of the system parameters are not crucial for the algorithm proposed to return a successful condensation protocol and the values used in the following, specified in the SM [25], are within the experimentally accessible ranges discussed above. The energies of the reservoir spins are set in resonance with different energy-level distances in the system such that the peaks of their spectral density approximate the overall connectivity sketched in Fig. 2(a), ensuring that every state is reachable via quantum jumps. The energy-spacing–to–spin association is chosen by verifying numerically that strong matrix elements $|M_{ij}^{(\ell)}|$ are attained.

We solve Eqs. (7) for the control variables z by targeting BS into a chosen set of three modes $\{|0\rangle, |2\rangle, |3\rangle\}$, with target condensate fractions $[\boldsymbol{\nu}_{S,0}, \boldsymbol{\nu}_{S,2}, \boldsymbol{\nu}_{S,3}] = [1/10, 3/10, 6/10]$, finding the control values χ_ℓ and the asymmetry matrix depicted in Fig. 2(b). The latter features the loop structure of Fig. 1(b) (top) within the set of selected states (red arrows), needed to sustain BS. To verify the validity of the effective rates (6) derived, we compare in Fig. 2(d) the single-particle dynamics given by those rates with the master equation (3), confirming good agreement. The achievement of the desired BS pattern in the steady state is shown in Fig. 2(e), where saturation of nonselected states starts for $N \gtrsim 30$ and the target fractions are reproduced faithfully already for $N = 100$. The steady-state occupations are computed numerically here with different methods corresponding to the approximation layers used in designing the control protocol (recapitulated in [25]), to confirm their reliability: solution of the asymptotic large-N theory of Eq. (2) underpinning the algorithm (7) via linear programming [33] (dashed lines), long-time propagation of the mean-field kinetic equations (solid lines), and long-time propagation of the populations of $\hat{\rho}_S(t)$ from Eq. (1) via a quasiexact Monte Carlo quantum-trajectory-type unraveling [21] (circles, averaged over 10^3 trajectories). Due to the bosonic enhancement in the many-body rates, the evolution converges rapidly to its BS steady state [Fig. 2(f)]. The depletion of nonselected states takes place within a few tens of tunneling times for $N = 50$ (solid lines) and faster and faster as N increases [$N = 500$ in Fig. 2(f), dashed lines]. By exploring different connectivities through different energy-spacing–to–spin associations and solving for z, protocols giving selection into any triplet of states, with the same occupation fractions as above, are also found [25]. Condensation in individual states can also be achieved; see Fig. 2(c), which shows examples with $|1\rangle$ and $|2\rangle$.

To exemplify controlled selection into more than three states, we target five modes of a ten-site chain. The reservoir spins realize rate asymmetries A_{ij} for which each target mode is strongly connected to at least two other selected states. Choosing selected states $\{|2\rangle, |4\rangle, |5\rangle, |7\rangle, |9\rangle\}$ with equal occupancy and solving Eqs. (7) for z gives the asymmetry matrix of Fig. 3(a), where we find a rate structure of the type of Fig. 1(b) (bottom) within S. The target BS pattern is successfully attained [Fig. 3(b)]. The examples considered represent ideal system sizes for potential implementation: They are sufficient to demonstrate the desired effect while being close to setups already realized [38,39]. Also, in view of potential applications as they are discussed below, larger system sizes do not provide an advantage. For much larger chain lengths, we expect that inducing fully arbitrary condensation patterns will become increasingly challenging. As the spectrum becomes denser for increasing length, the transitions induced by the artificial baths will become less selective. Moreover, the number of level spacings grows much faster than the number of control parameters, assuming the use of one reservoir spin per resonator. Still, the control method proposed here may be used to drive BS into states within a certain

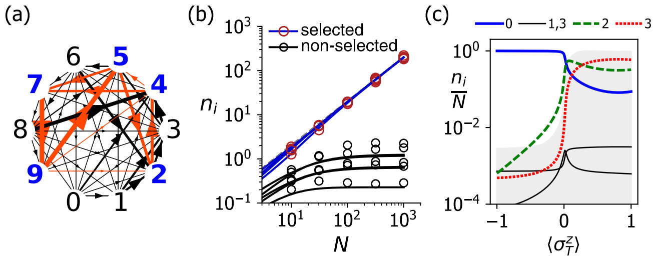

FIG. 3. (a) Asymmetry matrix for a selection of five modes (blue) in a ten-site chain; transitions within S are colored red. (b) Achievement of BS with requested equal occupancy (solid lines represent the results of mean-field theory and circles the average of 500 quantum trajectories. (c) BEC pattern vs expectation value $\langle\hat{\sigma}_T^z\rangle$ of the trigger spin for $N = 10^2$. The gray area indicates the total value of the heat current $-\sum_{\ell\in B_X} j_h^{(\ell)}$ induced in the energy-extracting artificial baths (denoted by the set B_X), normalized by its maximum.

energy window of finite width, rather than sharply in individual states.

We assumed until now negligible particle loss, namely, that the resonators' relaxation is much slower than the engineered dissipation. In the SM [25] we analyze the impact of weak losses and the use of spin reservoirs realizing particle pumps to counteract them. If the total mean particle number is kept large, BS is, to a good approximation, solely dictated by the matrix A, rather than by pump and loss. It is thus still successfully controlled with the above methods. This is easily explained by the fact that BS derives from terms in the mean-field equation that are quadratic in n_i, whereas pump and loss enter linearly. For the same reason, the BS steady state is attained well before substantial losses occur. Pump and loss may also be used as additional control parameters.

A condensate switch. Realizing nonequilibrium phases which are *per se* robust, but tuned to be sensitive to few selected parameters, is a promising resource for, e.g., amplification and sensing. We can use the ability to control BS to design similar conditions in the Bose condenser. The system can be tuned to a transition point between two (or more) BS configurations such that the state of an additional "trigger" system coupled to it determines which condensation pattern arises. For instance, in the five-site device of Fig. 2(a), the three-state BS turns into ground-state condensation if the quantum jump governed by the third reservoir spin is forced towards the ground state. Consider then a coupling of the spin's detuning δ_3 to an additional trigger spin T, through the Hamiltonian $\hat{H} = \delta_3(r_3\hat{\sigma}_3^x + \hat{\sigma}_3^z\hat{\sigma}_T^z) + \omega_T\hat{\sigma}_T^z/2$. Enforcing $|\mathcal{E}_3| \approx |E_{20}|$, the bosonic steady state then depends on the state of T, through the renormalization of δ_3 by $\langle\hat{\sigma}_T^z\rangle$. Depending on whether $\langle\hat{\sigma}_T^z\rangle = \pm 1$, the chain will exhibit either three-state or ground-state selection, as numerically verified in Fig. 3(c). A similar device may be used, for instance, as a switch that activates or deactivates the transport of macroscopic energy currents through the system. Indeed, the heat current $j_h^{(\ell)}$ generated in the system by the coupling to the ℓth artificial bath is given, within the mean-field theory, by $j_h^{(\ell)} = \mathrm{tr}(\dot{\hat{\rho}}_S\hat{H}_S) \approx \sum_{ij}(E_j - E_i)n_i(n_j + 1)R_{ji}^{(\ell)}$ [20]. The current is bosonically enhanced (quadratic in the n_i) for transitions between selected states, while it is only linearly enhanced for transitions between a selected and a nonselected state. When multiple condensates are present, the system has thus the ability to absorb and emit much more energy at large particle numbers. This feature may be of particular interest for the use of the BS system as a junction ruling quantum heat transport in a more complex device or as an artificial bath with a highly structured spectral density. The heat-current enhancement is shown in Fig. 3(c) for the five-site Bose condenser (gray shading) as the system passes from a single-condensate to a three-condensate phase. An interesting perspective in this context is also the classification of such nonequilibrium phase transitions among BS patterns. The latter may be distinguished in terms of the topology of the quantum-jump network, for instance, exploiting the mathematical similarity between the BS asymmetry-matrix theory and Lotka-Volterra systems in evolutionary game theory [53].

Conclusion. We showed how nonequilibrium BEC can be controlled via the coupling to engineered quantum baths. We designed a physical setup, implementable, e.g., in superconducting-circuit architectures, granting a handle on the condensate location and fragmentation, which can thus be shaped on demand. These results pave the way to applications in the control of heat transport, amplification, and quantum bath engineering. Combined with topologically nontrivial band structures, controlled selection may facilitate edge-mode detection [54] or realize topological laserlike [55,56] steady states.

Acknowledgment. This research was funded by the Deutsche Forschungsgemeinschaft (German Research Foundation) via the Research Unit FOR 2414 through Project No. 277974659.

[1] J. Bloch, I. Carusotto, and M. Wouters, Non-equilibrium Bose–Einstein condensation in photonic systems, Nat. Rev. Phys. **4**, 470 (2022).

[2] J. Klaers, J. Schmitt, F. Vewinger, and M. Weitz, Bose–Einstein condensation of photons in an optical microcavity, Nature (London) **468**, 545 (2010).

[3] J. Schmitt, T. Damm, D. Dung, F. Vewinger, J. Klaers, and M. Weitz, Thermalization kinetics of light: From laser dynamics to equilibrium condensation of photons, Phys. Rev. A **92**, 011602(R) (2015).

[4] B. T. Walker, L. C. Flatten, H. J. Hesten, F. Mintert, D. Hunger, A. A. P. Trichet, J. M. Smith, and R. A. Nyman, Driven-dissipative non-equilibrium Bose–Einstein condensation of less than ten photons, Nat. Phys. **14**, 1173 (2018).

[5] H. J. Hesten, R. A. Nyman, and F. Mintert, Decondensation in nonequilibrium photonic condensates: When less is more, Phys. Rev. Lett. **120**, 040601 (2018).

[6] D. Vorberg, R. Ketzmerick, and A. Eckardt, Unified theory for excited-state, fragmented, and equilibriumlike Bose

condensation in pumped photonic many-body systems, Phys. Rev. A **97**, 063621 (2018).

[7] B. T. Walker, H. J. Hesten, H. S. Dhar, R. A. Nyman, and F. Mintert, Noncritical slowing down of photonic condensation, Phys. Rev. Lett. **123**, 203602 (2019).

[8] M. Vlaho and A. Eckardt, Nonequilibrium mode competition in a pumped dye-filled cavity, Phys. Rev. A **104**, 063709 (2021).

[9] L. V. Butov, A. C. Gossard, and D. S. Chemla, Macroscopically ordered state in an exciton system, Nature (London) **418**, 751 (2002).

[10] A. A. High, J. R. Leonard, A. T. Hammack, M. M. Fogler, L. V. Butov, A. V. Kavokin, K. L. Campman, and A. C. Gossard, Spontaneous coherence in a cold exciton gas, Nature (London) **483**, 584 (2012).

[11] M. Alloing, M. Beian, M. Lewenstein, D. Fuster, Y. González, L. González, R. Combescot, M. Combescot, and F. Dubin, Evidence for a Bose-Einstein condensate of excitons, Europhys. Lett. **107**, 10012 (2014).

[12] L. S. Dang, D. Heger, R. André, F. Bœuf, and R. Romestain, Stimulation of polariton photoluminescence in semiconductor microcavity, Phys. Rev. Lett. **81**, 3920 (1998).

[13] H. Deng, G. Weihs, C. Santori, J. Bloch, and Y. Yamamoto, Condensation of semiconductor microcavity exciton polaritons, Science **298**, 199 (2002).

[14] J. Kasprzak, M. Richard, S. Kundermann, A. Baas, P. Jeambrun, J. M. J. Keeling, F. M. Marchetti, M. H. Szymańska, R. André, J. L. Staehli, V. Savona, P. B. Littlewood, B. Deveaud, and L. S. Dang, Bose–Einstein condensation of exciton polaritons, Nature (London) **443**, 409 (2006).

[15] R. Balili, V. Hartwell, D. Snoke, L. Pfeiffer, and K. West, Bose-Einstein condensation of microcavity polaritons in a trap, Science **316**, 1007 (2007).

[16] H. Deng, H. Haug, and Y. Yamamoto, Exciton-polariton Bose-Einstein condensation, Rev. Mod. Phys. **82**, 1489 (2010).

[17] T. Byrnes, N. Y. Kim, and Y. Yamamoto, Exciton–polariton condensates, Nat. Phys. **10**, 803 (2014).

[18] F. Baboux, L. Ge, T. Jacqmin, M. Biondi, E. Galopin, A. Lemaître, L. Le Gratiet, I. Sagnes, S. Schmidt, H. E. Türeci, A. Amo, and J. Bloch, Bosonic condensation and disorder-induced localization in a flat band, Phys. Rev. Lett. **116**, 066402 (2016).

[19] E. Wertz, L. Ferrier, D. D. Solnyshkov, R. Johne, D. Sanvitto, A. Lemaître, I. Sagnes, R. Grousson, A. V. Kavokin, P. Senellart, G. Malpuech, and J. Bloch, Spontaneous formation and optical manipulation of extended polariton condensates, Nat. Phys. **6**, 860 (2010).

[20] D. Vorberg, W. Wustmann, R. Ketzmerick, and A. Eckardt, Generalized Bose-Einstein condensation into multiple states in driven-dissipative systems, Phys. Rev. Lett. **111**, 240405 (2013).

[21] D. Vorberg, W. Wustmann, H. Schomerus, R. Ketzmerick, and A. Eckardt, Nonequilibrium steady states of ideal bosonic and fermionic quantum gases, Phys. Rev. E **92**, 062119 (2015).

[22] A. Schnell, D. Vorberg, R. Ketzmerick, and A. Eckardt, High-temperature nonequilibrium Bose condensation induced by a hot needle, Phys. Rev. Lett. **119**, 140602 (2017).

[23] A. Schnell, R. Ketzmerick, and A. Eckardt, On the number of Bose-selected modes in driven-dissipative ideal Bose gases, Phys. Rev. E **97**, 032136 (2018).

[24] A. Schnell, L.-N. Wu, A. Widera, and A. Eckardt, Floquet-heating-induced Bose condensation in a scarlike mode of an open driven optical-lattice system, Phys. Rev. A **107**, L021301 (2023).

[25] See Supplemental Material at http://link.aps.org/supplemental/10.1103/PhysRevA.110.L021701, where we provide (i) a recapitulation of the models and numerical methods used, including the approximations involved; (ii) a discussion about asymmetry-matrix structures compatible with Bose selection, in relation to Fig. 1(b); (iii) the derivation of the single-particle quantum-jump rates and rate-asymmetry matrices induced by the artificial baths; (iv) the specific values of the system parameters used in the simulations reported in the text and further examples; (v) additional considerations concerning the experimental feasibility of the proposed setup; and (vi) the impact of particle pump and loss from the bosonic system and which includes Refs. [26–32].

[26] H. J. Carmichael, *Statistical Methods in Quantum Optics 1: Master Equations and Fokker-Planck Equations* (Springer, Berlin, 1999).

[27] A. W. Tucker, in *Linear Inequalities and Related Systems*, edited by H. W. Kuhn and A. W. Tucker (Princeton University Press, Princeton, 1957), pp. 3–18.

[28] P. Virtanen, R. Gommers, T. E. Oliphant, M. Haberland, T. Reddy, D. Cournapeau, E. Burovski, P. Peterson, W. Weckesser, J. Bright, S. J. van der Walt, M. Brett, J. Wilson, K. J. Millman, N. Mayorov, A. R. J. Nelson, E. Jones, R. Kern, E. Larson, C. J. Carey *et al.*, SciPy 1.0: Fundamental algorithms for scientific computing in Python, Nat. Methods **17**, 261 (2020).

[29] A. J. Kollár, M. Fitzpatrick, and A. A. Houck, Hyperbolic lattices in circuit quantum electrodynamics, Nature (London) **571**, 45 (2019).

[30] F. Arute, K. Arya, R. Babbush, D. Bacon, J. C. Bardin, R. Barends, R. Biswas, S. Boixo, F. G. S. L. Brandao, D. A. Buell, B. Burkett *et al.*, Quantum supremacy using a programmable superconducting processor, Nature (London) **574**, 505 (2019).

[31] J. Majer, J. M. Chow, J. M. Gambetta, B. R. J. Jens Koch, J. A. Schreier, L. Frunzio, D. I. Schuster, A. A. Houck, A. Wallraff, A. Blais, M. H. Devoret, S. M. Girvin, and R. J. Schoelkopf, Coupling superconducting qubits via a cavity bus, Nature (London) **449**, 443 (2007).

[32] M. Hofheinz, E. M. Weig, M. Ansmann, R. C. Bialczak, E. Lucero, M. Neeley, A. D. O'Connell, H. Wang, J. M. Martinis, and A. N. Cleland, Generation of Fock states in a superconducting quantum circuit, Nature (London) **454**, 310 (2008).

[33] J. Knebel, M. F. Weber, T. Krüger, and E. Frey, Evolutionary games of condensates in coupled birth–death processes, Nat. Commun. **6**, 6977 (2015).

[34] J. Knebel, T. Krüger, M. F. Weber, and E. Frey, Coexistence and survival in conservative Lotka-Volterra networks, Phys. Rev. Lett. **110**, 168106 (2013).

[35] P. Krantz, M. Kjaergaard, F. Yan, T. P. Orlando, S. Gustavsson, and W. D. Oliver, A quantum engineer's guide to superconducting qubits, Appl. Phys. Rev. **6**, 021318 (2019).

[36] A. Blais, A. L. Grimsmo, S. M. Girvin, and A. Wallraff, Circuit quantum electrodynamics, Rev. Mod. Phys. **93**, 025005 (2021).

[37] P. Roushan, C. Neill, J. Tangpanitanon, V. M. Bastidas, A. Megrant, R. Barends, Y. Chen, Z. Chen, B. Chiaro, A. Dunsworth, A. Fowler, B. Foxen, M. Giustina, E. Jeffrey, J. Kelly, E. Lucero, J. Mutus, M. Neeley, C. Quintana, D. Sank *et al.*, Spectroscopic signatures of localization with interacting photons in superconducting qubits, Science **358**, 1175 (2017).

[38] Z. Yan, Y.-R. Zhang, M. Gong, Y. Wu, Y. Zheng, S. Li, C. Wang, F. Liang, J. Lin, Y. Xu *et al.*, Strongly correlated quantum walks with a 12-qubit superconducting processor, Science **364**, 753 (2019).
[39] R. Ma, B. Saxberg, C. Owens, N. Leung, Y. Lu, J. Simon, and D. I. Schuster, A dissipatively stabilized Mott insulator of photons, Nature (London) **566**, 51 (2019).
[40] I. Carusotto, A. A. Houck, A. J. Kollár, P. Roushan, D. I. Schuster, and J. Simon, Photonic materials in circuit quantum electrodynamics, Nat. Phys. **16**, 268 (2020).
[41] D. Marcos, A. Tomadin, S. Diehl, and P. Rabl, Photon condensation in circuit quantum electrodynamics by engineered dissipation, New J. Phys. **14**, 055005 (2012).
[42] X. Mi, A. A. Michailidis, S. Shabani, K. C. Miao, P. V. Klimov, J. Lloyd, E. Rosenberg, R. Acharya, I. Aleiner, T. I. Andersen *et al.*, Stable quantum-correlated many-body states through engineered dissipation, Science **383**, 1332 (2024).
[43] A. Blais, R.-S. Huang, A. Wallraff, S. M. Girvin, and R. J. Schoelkopf, Cavity quantum electrodynamics for superconducting electrical circuits: An architecture for quantum computation, Phys. Rev. A **69**, 062320 (2004).
[44] J. Koch, T. M. Yu, J. Gambetta, A. A. Houck, D. I. Schuster, J. Majer, A. Blais, M. H. Devoret, S. M. Girvin, and R. J. Schoelkopf, Charge-insensitive qubit design derived from the Cooper pair box, Phys. Rev. A **76**, 042319 (2007).
[45] F. Swiadek, R. Shillito, P. Magnard, A. Remm, C. Hellings, N. Lacroix, Q. Ficheux, D. C. Zanuz, G. J. Norris, A. Blais, S. Krinner, and A. Wallraff, Enhancing dispersive readout of superconducting qubits through dynamic control of the dispersive shift: Experiment and theory, arXiv:2307.07765.
[46] Y. Chen, C. Neill, P. Roushan, N. Leung, M. Fang, R. Barends, J. Kelly, B. Campbell, Z. Chen, B. Chiaro, A. Dunsworth, E. Jeffrey, A. Megrant, J. Y. Mutus, P. J. J. O'Malley, C. M. Quintana, D. Sank, A. Vainsencher, J. Wenner, T. C. White *et al.*, Qubit architecture with high coherence and fast tunable coupling, Phys. Rev. Lett. **113**, 220502 (2014).
[47] P. Roushan, C. Neill, A. Megrant, Y. Chen, R. Babbush, R. Barends, B. Campbell, Z. Chen, B. Chiaro, A. Dunsworth, A. Fowler, E. Jeffrey, J. Kelly, E. Lucero, J. Mutus, P. J. J. O'Malley, M. Neeley, C. Quintana, D. Sank, A. Vainsencher *et al.*, Chiral ground-state currents of interacting photons in a synthetic magnetic field, Nat. Phys. **13**, 146 (2017).
[48] K. W. Murch, U. Vool, D. Zhou, S. J. Weber, S. M. Girvin, and I. Siddiqi, Cavity-assisted quantum bath engineering, Phys. Rev. Lett. **109**, 183602 (2012).
[49] S. Hacohen-Gourgy, V. V. Ramasesh, C. De Grandi, I. Siddiqi, and S. M. Girvin, Cooling and autonomous feedback in a Bose-Hubbard chain with attractive interactions, Phys. Rev. Lett. **115**, 240501 (2015).
[50] E. Kapit, The upside of noise: Engineered dissipation as a resource in superconducting circuits, Quantum Sci. Technol. **2**, 033002 (2017).
[51] F. Petiziol and A. Eckardt, Cavity-based reservoir engineering for Floquet-engineered superconducting circuits, Phys. Rev. Lett. **129**, 233601 (2022).
[52] H.-P. Breuer and F. Petruccione, *The Theory of Open Quantum Systems* (Oxford University Press, Oxford, 2007).
[53] P. M. Geiger, J. Knebel, and E. Frey, Topologically robust zero-sum games and Pfaffian orientation: How network topology determines the long-time dynamics of the antisymmetric Lotka-Volterra equation, Phys. Rev. E **98**, 062316 (2018).
[54] S. Furukawa and M. Ueda, Excitation band topology and edge matter waves in Bose–Einstein condensates in optical lattices, New J. Phys. **17**, 115014 (2015).
[55] M. A. Bandres, S. Wittek, G. Harari, M. Parto, J. Ren, M. Segev, D. N. Christodoulides, and M. Khajavikhan, Topological insulator laser: Experiments, Science **359**, eaar4005 (2018).
[56] G. Harari, M. A. Bandres, Y. Lumer, M. C. Rechtsman, Y. D. Chong, M. Khajavikhan, D. N. Christodoulides, and M. Segev, Topological insulator laser: Theory, Science **359**, eaar4003 (2018).